

# Ubiquitin Backbone Motion Studied via $\text{NH}^{\text{N}}-\text{C}'\text{C}_{\alpha}$ Dipolar–Dipolar and $\text{C}'-\text{C}'\text{C}_{\alpha}/\text{NH}^{\text{N}}$ CSA–Dipolar Cross-Correlated Relaxation

Teresa Carlomagno,<sup>†</sup> Marcus Maurer, Mirko Hennig,<sup>†</sup> and Christian Griesinger\*

Contribution from the Institut für Organische Chemie, Universität Frankfurt, Marie-Curie Strasse 11, D-60439 Frankfurt, Germany

Received October 28, 1999. Revised Manuscript Received February 14, 2000

**Abstract:** While it is recognized that protein side chains undergo large reorientations, very little is known about the extent and the nature of the motions within the protein backbone. These motions can be studied by chemical shift anisotropy (CSA)–dipolar cross-correlated relaxation rates, the interpretation of which relies on prior knowledge of the CSA principal axis values and directions. Alternatively, dipolar–dipolar cross-correlated relaxation rates can be used. Here we propose a CT-HNCO experiment to measure the sum of the two  $\text{C}'\text{C}_{\alpha}/\text{NC}_{\alpha}$  dipolar– $\text{NH}^{\text{N}}/\text{C}'\text{H}^{\text{N}}$  dipolar cross-correlated relaxation rates. At the same time the experiment gives access to the cross-correlated relaxation rates between  $\text{C}'$  CSA and the  $\text{NH}^{\text{N}}$  or  $\text{C}'\text{C}_{\alpha}$  dipoles. The complete set of three cross-correlated relaxation rates, measured for the protein ubiquitin, is interpreted in terms of the Gaussian axial fluctuation model of motion. This model provides a good framework for the description of the motions of peptide planes in  $\alpha$ -helical and turn regions, while a poor fitting of the cross-correlated relaxation data is obtained for  $\beta$ -sheet regions. The cross-correlated relaxation rates for the  $\alpha$ -helix peptide planes 23–34 are similar, and their characteristic values suggest the possibility of a concerted motion of the helix or systematic changes in the carbonyl CSA principal axis values and directions.

## Introduction

Conformational dynamics influences both the properties and the biological functions of biomacromolecules. Molecular motions can be assessed experimentally by analyzing NMR spin relaxation rates.<sup>1</sup> Several attempts based on autocorrelated relaxation rates aimed at developing models for local motions of peptide planes in proteins.<sup>1b–e</sup> Since such motions are in general anisotropic, they can be characterized best by physical observables which are very sensitive to the direction of motion, like cross-correlated relaxation rates. Cross-correlated relaxation arises from the interference of two relaxation mechanisms (chemical shift anisotropy (CSA), dipole–dipole interaction), which are described by tensors in the three-dimensional space. The order parameter of a cross-correlated relaxation rate contains information both on the relative directions of these tensors in absence of internal motion and on the correlated motions of the tensors in the presence of internal reorientations. In moieties with fixed geometry, such as peptide planes, cross-correlated relaxation data allow access to information on dynamics in a unique way because of their high sensitivity to the anisotropy of motion.

Recently, a number of liquid-state NMR experiments have been developed to derive cross-correlated relaxation rates between either two dipolar,<sup>2a–e,i,j</sup> a dipolar and a CSA,<sup>2f–h,j</sup> or

two CSA relaxation mechanisms<sup>2i</sup> in proteins. To interpret CSA–dipolar cross-correlated relaxation rates with respect to protein backbone dynamics, assumptions must be made about the size and the orientation of  $^{13}\text{C}'$  and  $^{15}\text{N}$  CSA tensors in the molecular frame. Both the size and the orientation of these tensors may vary for each amino acid residue due to different secondary structure elements and associated hydrogen-bonding patterns. To become independent of these variations in CSA principal axis values and directions, we measure an additional cross-correlated relaxation rate, based on two dipolar interactions, which depends only on unambiguous physical constants, such as bond lengths. The topology of the peptide plane allows for a number of dipolar–dipolar cross-correlated relaxation rates, whose amplitudes relative to that of the dipolar autocorrelated  $\text{NH}^{\text{N}}$  relaxation rate are reported in Table 1. Among these rates, the most accessible is  $\Gamma_{\text{C}'\text{C}_{\alpha},\text{NH}^{\text{N}}}^{\text{DD}/\text{DD}}$  between the  $\text{NH}^{\text{N}}$  and the  $\text{C}'\text{C}_{\alpha}$  dipole–dipole interactions, because of the favorable large one-bond couplings relative to the line width typically observed in biomacromolecules.  $\Gamma_{\text{C}'\text{C}_{\alpha},\text{NH}^{\text{N}}}^{\text{DD}/\text{DD}}$  cannot be separated from the  $\Gamma_{\text{C}'\text{H}^{\text{N}},\text{NC}_{\alpha}}^{\text{DD}/\text{DD}}$  cross-correlated relaxation rate, so the sum of the two rates has to be interpreted. In the absence of motion and assuming standard geometry of the peptide plane,<sup>3</sup>

\* Corresponding author. Tel.: +49-69-79829130. Fax: +49-69-79829128. E-mail address: cigr@org.chemie.uni-frankfurt.de. also at Max Planck Institute for Biophysical Chemistry, Am Fassberg 11, 37077 Göttingen, Germany.

<sup>†</sup> Present address: Department of Molecular Biology & The Skaggs Institute of Chemical Biology, The Scripps Research Institute, MB 33, 10550 North Torrey Pines Rd., La Jolla, CA 92037.

(1) (a) Palmer, A. G., III. *Curr. Opin. Struct. Biol.* **1997**, *7*, 732–737. (b) Engelke, J.; Ruterjans, H. *J. Biomol. NMR* **1997**, *9*, 63–78. (c) Allard, P.; Hard, T. *J. Magn. Reson. Ser. B* **1997**, *126*, 48–57. (d) Dayie, K. T.; Wagner, G. *J. Am. Chem. Soc.* **1997**, *119*, 7797–7806. (e) Lienin, S. F.; Bremi, T.; Brutscher, B.; Brüschweiler, R.; Ernst, R. R. *J. Am. Chem. Soc.* **1998**, *120*, 9870–9879. (f) Brüschweiler, R.; Case, D. A. *Prog. NMR Spectrosc.* **1994**, *26*, 27–58.

(2) (a) Reif, B.; Hennig, M.; Griesinger, C. *Science* **1997**, *276*, 1230–1233. (b) Reif, B.; Steinhagen, H.; Junker, B.; Reggelin, M.; Griesinger, C. *Angew. Chem., Int. Ed. Eng.* **1998**, *37*, 2006–2009. (c) Griesinger, C.; Hennig, M.; Marino, J. P.; Reif, B.; Schwalbe, H. In *Modern Techniques in Protein NMR*; Rama Krishna, N., Berliner, L. J., Eds.; Biological Magnetic Resonance 16; Plenum: London, 1998; pp 259–367. (d) Yang, D.; Kay, L. E. *J. Am. Chem. Soc.* **1998**, *120*, 9880–9887. (e) Yang, D.; Konrat, R.; Kay, L. E. *J. Am. Chem. Soc.* **1997**, *119*, 11938–11940. (f) Brutscher, B.; Skrynnikov, N. R.; Bremi, T.; Brüschweiler, R.; Ernst, R. R. *J. Magn. Reson.* **1998**, *130*, 346–351. (g) Fischer, M. W. F.; Zeng, L.; Pang, Y.; Hu, W.; Majumdar, A.; Zuiderweg, E. R. P. *J. Am. Chem. Soc.* **1997**, *119*, 12629–12642. (h) Pang, Y.; Wang, L.; Pellecchia, M.; Kurochkin, A. V.; Zuiderweg, E. R. P. *J. Biomol. NMR.* **1999**, *14*, 297–306. (i) Pellecchia, M.; Pang, Y.; Wang, L.; Kurochkin, A. V.; Kumar, A.; Zuiderweg, E. R. P. *J. Am. Chem. Soc.* **1999**, *121*, 9165–9170. (j) Chiapparini, E.; Pelupessy, P.; Ghose, R.; Bodenhausen, G. *J. Am. Chem. Soc.* **1999**, *121*, 6876–6883.

**Table 1.** Size in Hertz of Possible Dipolar–Dipolar Cross-Correlated Rates among the Atoms of a Peptide Plane Normalized to the Size of the  $\text{NH}^{\text{N}}$  Dipolar Autocorrelated Relaxation, Assuming Absence of Internal Motions<sup>a</sup>

	$\text{H}_i^{\text{N}}\text{N}_i$	$\text{H}_i^{\text{N}}\text{C}'_{i-1}$	$\text{H}_i^{\text{N}}\text{C}_{\alpha,i-1}$	$\text{H}_i^{\text{N}}\text{C}_{\alpha,i}$	$\text{C}'_{i-1}\text{C}_{\alpha,i-1}$	$\text{N}_i\text{C}_{\alpha,i-1}$	$\text{N}_i\text{C}_{\alpha,i}$
$\text{H}_i^{\text{N}}\text{N}_i$	1	−0.166	0.072	−0.138	−0.014	−0.010	−0.007
$\text{H}_i^{\text{N}}\text{C}'_{i-1}$	<b>−0.372</b>	0.116	0.028	−0.030	−0.035	0.001	−0.015
$\text{H}_i^{\text{N}}\text{C}_{\alpha,i-1}$	<b>−0.210</b>	<b>0.062</b>	0.035	−0.017	0.000	−0.003	−0.015
$\text{H}_i^{\text{N}}\text{C}_{\alpha,i}$	<b>−0.264</b>	<b>0.087</b>	<b>0.049</b>	0.070	0.003	−0.004	−0.018
$\text{C}'_{i-1}\text{C}_{\alpha,i-1}$	<b>0.204</b>	<b>0.068</b>	<b>0.004</b>	<b>0.054</b>	0.042	−0.003	−0.018
$\text{N}_i\text{C}_{\alpha,i-1}$	<b>0.020</b>	<b>−0.007</b>	<b>−0.004</b>	<b>−0.007</b>	<b>−0.004</b>	0.0004	0.000
$\text{N}_i\text{C}_{\alpha,i}$	<b>0.092</b>	<b>−0.030</b>	<b>−0.017</b>	<b>−0.024</b>	<b>−0.019</b>	<b>0.002</b>	0.008

<sup>a</sup> The values have been calculated assuming standard geometry of the peptide plane as derived by ref 3 in the upper part of the table, while the values in the lower part of the table (bold entries) have been calculated assuming that the two interfering relaxation mechanisms can be represented by parallel vectors.

$\Gamma_{\text{C}'_{\alpha}\text{C}_{\alpha}\text{NHN}}^{\text{DD/DD}}$  is close to zero (−0.106 Hz for  $\tau_c = 4.1$  ns; the maximum value of  $\Gamma_{\text{C}'_{\alpha}\text{C}_{\alpha}\text{NHN}}^{\text{DD/DD}}$  is to be expected for a *cis* conformation of the peptide bond and is equal to 1.546 Hz for  $\tau_c = 4.1$  ns), and  $\Gamma_{\text{C}'_{\text{HN}}\text{NC}_{\alpha}}^{\text{DD/DD}}$  is even smaller (0.009 Hz). Although, as will become clear in the following, the measurement of such small rates is rather inaccurate for proteins of small size, we expect that for proteins with higher molecular weight  $\Gamma_{\text{C}'_{\alpha}\text{C}_{\alpha}\text{NHN}}^{\text{DD/DD}}$  can be measured with the accuracy required for a rigorous quantitative analysis. Recently, the measurement of another dipolar–dipolar cross-correlated relaxation rate in the peptide plane,  $\Gamma_{\text{C}'_{\text{HN}}\text{NHN}}^{\text{DD/DD}}$ , has been proposed by others.<sup>21</sup>

In the following, we describe a method to measure the  $\Gamma_{\text{C}'_{\alpha}\text{C}_{\alpha}\text{NHN}}^{\text{DD/DD}} + \Gamma_{\text{C}'_{\text{HN}}\text{NHN}}^{\text{DD/DD}}$  rate, where the rate is extracted from the difference in intensity of multiplet lines. In addition, this experiment allows the measurement of two CSA–dipolar cross-correlated relaxation rates, namely  $\Gamma_{\text{N,NC}_{\alpha}}^{\text{CSA/DD}} + \Gamma_{\text{C}'_{\alpha}\text{C}_{\alpha}}^{\text{CSA/DD}}$  and  $\Gamma_{\text{C}'_{\text{HN}}\text{NHN}}^{\text{CSA/DD}} + \Gamma_{\text{N,C}'_{\alpha}}^{\text{CSA/DD}}$ . An interpretation of these three cross-correlated relaxation rates in terms of the Gaussian axial fluctuation (GAF) model<sup>4</sup> is shown for the protein ubiquitin, revealing particularly interesting observations in the helical region spanning residues 23–34.

## Theory

The two dipolar–dipolar cross-correlated relaxation rates are given by the following equations:

$$\Gamma_{\text{C}'_{\alpha}\text{C}_{\alpha}\text{NHN}} = \left(\frac{\mu_0}{4\pi}\right)^2 \frac{\hbar^2 \gamma_{\text{H}} \gamma_{\text{N}} \gamma_{\text{C}}^2}{r_{\text{NHN}}^3 r_{\text{C}'_{\alpha}\text{C}_{\alpha}}^3} J_{\text{C}'_{\alpha}\text{C}_{\alpha}\text{NHN}}(0)$$

$$J_{\text{C}'_{\alpha}\text{C}_{\alpha}\text{NHN}}(\omega) = \frac{2}{5} S_{\text{C}'_{\alpha}\text{C}_{\alpha}\text{NHN}}^2 \frac{\tau_c}{1 + \omega^2 \tau_c^2} + \frac{2}{5} (P_2(\cos \theta_{\text{C}'_{\alpha}\text{C}_{\alpha}\text{NHN}}) - S_{\text{C}'_{\alpha}\text{C}_{\alpha}\text{NHN}}^2) \frac{\tau_{\text{eff}}}{1 + \omega^2 \tau_{\text{eff}}^2}$$

$$\Gamma_{\text{C}'_{\text{HN}}\text{NC}_{\alpha}} = \left(\frac{\mu_0}{4\pi}\right)^2 \frac{\hbar^2 \gamma_{\text{H}} \gamma_{\text{N}} \gamma_{\text{C}}^2}{r_{\text{C}'_{\text{HN}}}^3 r_{\text{NC}_{\alpha}}^3} J_{\text{C}'_{\text{HN}}\text{NC}_{\alpha}}(0)$$

$$J_{\text{C}'_{\text{HN}}\text{NC}_{\alpha}}(\omega) = \frac{2}{5} S_{\text{C}'_{\text{HN}}\text{NC}_{\alpha}}^2 \frac{\tau_c}{1 + \omega^2 \tau_c^2} + \frac{2}{5} (P_2(\cos \theta_{\text{C}'_{\text{HN}}\text{NC}_{\alpha}}) - S_{\text{C}'_{\text{HN}}\text{NC}_{\alpha}}^2) \frac{\tau_{\text{eff}}}{1 + \omega^2 \tau_{\text{eff}}^2}$$

(3) Creighton, T. E. *Proteins: Structures and Molecular Properties*; W. H. Freeman and Co.: New York, 1993.

(4) (a) Bremi, T.; Brüschweiler, R.; Ernst, R. R. *J. Am. Chem. Soc.* **1997**, *119*, 4272–4284. (b) Bremi, T.; Brüschweiler, R. *J. Am. Chem. Soc.* **1997**, *119*, 6672–6673.

where  $\gamma_{\text{H}}$ ,  $\gamma_{\text{C}}$ , and  $\gamma_{\text{N}}$  are the gyromagnetic ratios of proton, carbon, and nitrogen, respectively,  $r_{ij}$  is the distance between atom  $i$  and atom  $j$ ,  $S_{ij,kl}$  is the order parameter relative to the correlated motions of vector  $ij$  (distance vector between atom  $i$  and atom  $j$ ) and vector  $kl$  (distance vector between atom  $k$  and atom  $l$ );  $\theta_{ij,kl}$  is the projection angle between the vectors  $ij$  and  $kl$ ,  $P_2(x) = (3x^2 - 1)/2$ , and  $\tau_{\text{eff}}^{-1} = \tau_c^{-1} + \tau_e^{-1}$ , with  $\tau_e$  being the correlation time for internal motions. Similar expressions for  $\Gamma_{\text{N,NC}_{\alpha}}^{\text{CSA/DD}} + \Gamma_{\text{C}'_{\alpha}\text{C}_{\alpha}}^{\text{CSA/DD}}$  and  $\Gamma_{\text{C}'_{\text{HN}}\text{NHN}}^{\text{CSA/DD}} + \Gamma_{\text{N,C}'_{\alpha}}^{\text{CSA/DD}}$  have been given by others.<sup>2f,g</sup>

Any cross-correlated relaxation rate, due to the interference of two relaxation mechanisms represented by vectors  $ij$  and  $kl$ , is characterized by an order parameter  $S_{ij,kl}$ . This can be calculated by assuming a GAF model of motion,<sup>4</sup> according to the following:

$$S_{ij,kl}^2 = \frac{4\pi}{5} \sum_{m,p,p',q,q'=-2}^2 (-i)^{p-p'} e^{-\sigma_{\alpha}^2 m^2} e^{-\sigma_{\beta}^2 (p^2 + p'^2)/2} e^{-\sigma_{\gamma}^2 (q^2 + q'^2)/2} d_{pm}^{(2)}\left(\frac{\pi}{2}\right) d_{p'm}^{(2)}\left(\frac{\pi}{2}\right) d_{qp}^{(2)}\left(\frac{\pi}{2}\right) d_{q'p'}^{(2)}\left(\frac{\pi}{2}\right) Y_{2q}(\Omega_{ij}) Y_{2q'}^*(\Omega_{kl}) \quad (2)$$

where  $\sigma_{\alpha}$ ,  $\sigma_{\beta}$ , and  $\sigma_{\gamma}$  are the amplitudes of the Gaussian distributions of motions around three perpendicular axes  $\alpha$ ,  $\beta$ , and  $\gamma$ ,  $d^{(2)}$  are the Wigner rotation matrix elements,  $Y(\Omega)$  are the spherical harmonic functions, and  $\Omega(ij/kl)$  are the polar coordinates of vector  $ij/kl$ .

## Methods

The experiment for the measurement of the dipolar–dipolar  $\Gamma_{\text{C}'_{\alpha}\text{C}_{\alpha}\text{NHN}}^{\text{DD/DD}} + \Gamma_{\text{C}'_{\text{HN}}\text{NHN}}^{\text{DD/DD}}$  cross-correlated relaxation rate in proteins is a CT-HNCO type correlation experiment (Figure 1): during the constant time  $T$  both DQ and ZQ coherences of N and C' nuclei are present. Because the chemical shift of the nitrogen is refocused by the first and third nitrogen inversion pulse during the constant time  $T$ , DQ ( $\text{N}^+\text{C}^+$ ,  $\text{N}^-\text{C}^-$ ) and ZQ ( $\text{N}^-\text{C}^+$ ,  $\text{N}^+\text{C}^-$ ) coherences appear at the same frequency, namely the carbonyl one. This results in a signal-to-noise gain of  $\sqrt{2}$  with respect to an experiment, where DQ and ZQ coherences are acquired separately.<sup>1c</sup> Suppression of <sup>15</sup>N chemical shift evolution also refocuses the two scalar couplings  $J_{\text{N}'_{\alpha}i-1}$  and  $J_{\text{N}'_{\alpha}i}$ . This is particularly important, because the evolution of these scalar couplings would result in an additional splitting of  $\sim 11$  Hz on all four lines of the multiplet, seriously affecting the achievable resolution. The large one-bond  $J_{\text{NH}^{\text{N}}}$  coupling evolves during  $t_1$  as well as the  $J_{\text{C}'_{\alpha}\text{C}_{\alpha}}$  coupling. The two  $\pi$  <sup>1</sup>H pulses during the constant time  $T$  suppress the effect of  $\Gamma_{\text{N,NHN}}^{\text{CSA/DD}}$ . To a first-order approximation, the evolution times of all the possible dipolar–dipolar or CSA–dipolar cross-correlated relaxation rates involving nuclei in the peptide plane are reported in Table 2. As explained in detail elsewhere,<sup>2a-c</sup> the four lines of the multiplet deriving from the  $J_{\text{NH}^{\text{N}}}$  and the  $J_{\text{C}'_{\alpha}\text{C}_{\alpha}}$  couplings are affected differently by the rates summarized in Table 2. If the first and the second indexes

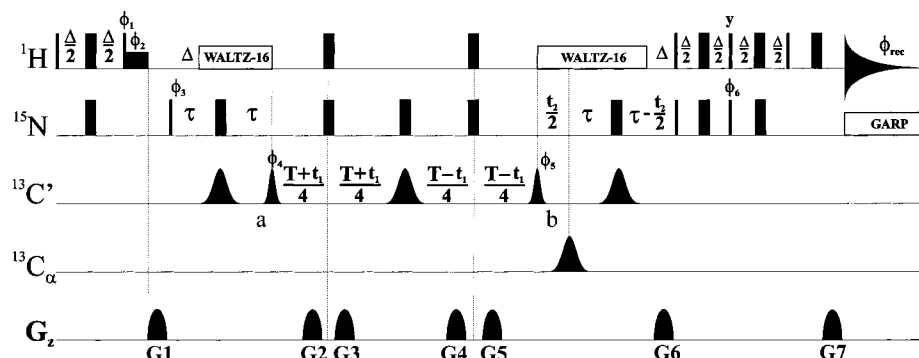


**Figure 1.** Pulse sequence for the measurement of  $\Gamma_{C'_{\alpha},NH^N}^{DD/DD} + \Gamma_{C'_{\alpha},NH^N}^{DD/DD}$ ,  $\Gamma_{N,NC_{\alpha}}^{CSA/DD} + \Gamma_{C',C'_{\alpha}}^{CSA/DD}$ , and  $\Gamma_{C',NH^N}^{CSA/DD} + \Gamma_{N,C'_{\alpha}}^{CSA/DD}$ . The sequence is an HNCOC correlation with the following parameters values:  $\tau = 13.5$  ms;  $\Delta = 5.4$  ms;  $\phi_1 = y$ ;  $\phi_2 = -x$ ;  $\phi_3 = x$ ,  $-x$ ;  $\phi_4 = 2x$ ,  $2(-x)$ ;  $\phi_5 = 4x$ ,  $4(-x)$ ;  $\phi_6 = y$ ;  $\phi_{rec} = (x, -x, -x, x, -x, x, x, -x)$ ;  $G2 = G3 = G4 = G5$ ;  $G6 = (\gamma_H/\gamma_N)G7$ . All phases not explicitly reported are equal to  $x$ . Quadrature is achieved in  $t_1$  by States-TPPI on  $\phi_4$ , and in  $t_2$  by adding and subtracting two fids acquired with  $\phi_6 = y$ ,  $G6 = A$  and  $\phi_6 = -y$ ,  $G6 = -A$ , respectively.  $^{13}C$  spins are irradiated with selective pulses ( $G4(90^\circ) = 512 \mu s$ ;  $Q3(180^\circ) = 548.6 \mu s$ ). The field strength for proton decoupling equals 4.1 kHz, for nitrogen decoupling during acquisition 1.0 kHz. The proton carrier is on water. The pulse with phase  $\phi_2$  is a low-power selective  $\pi/2$  pulse of duration 2 ms. Five 2D  $C'H$  correlations with different constant time values have been acquired ( $T = 50, 70, 90, 110$ , and  $130$  ms) consisting of a total of  $128(t_1) \times 1024(t_2)$  complex points per experiment. After linear prediction and zero-filling the final matrixes consist of  $512(\omega_1) \times 2048(\omega_2)$  points.

**Table 2.** Evolution Times of the Various Cross-Correlated Relaxation Rates during the Constant Time  $T$  of the Pulse Sequence of Figure 1

$\Gamma_{N,NH^N}^{CSA/DD}$	0	$\Gamma_{C',NH^N}^{CSA/DD}$	$T$	$\Gamma_{NH^N,C'_{\alpha}}^{DD/DD}$	0
$\Gamma_{N,C'_{\alpha}}^{CSA/DD}$	$T$	$\Gamma_{C',C'_{\alpha}}^{CSA/DD}$	0	$\Gamma_{NH^N,C'_{\alpha}}^{DD/DD}$	0
$\Gamma_{N,C'_{\alpha}}^{CSA/DD}$	0	$\Gamma_{C',NC_{\alpha}}^{CSA/DD}$	0	$\Gamma_{C'_{\alpha},NH^N}^{DD/DD}$	0
$\Gamma_{N,NC_{\alpha}}^{CSA/DD}$	$T$	$\Gamma_{C',C'_{\alpha}}^{DD/DD}$	$T$	$\Gamma_{C'_{\alpha},C'_{\alpha}}^{DD/DD}$	0
$\Gamma_{C',C'_{\alpha}}^{CSA/DD}$	$T$	$\Gamma_{NC_{\alpha},C'_{\alpha}}^{DD/DD}$	$T$	$\Gamma_{C'_{\alpha},C'_{\alpha}}^{DD/DD}$	0

associated with DQ/ZQ  $NC'$  coherences characterize the spin state of the  $H^N$  and the  $C_{\alpha}$  spin, respectively, the individual relaxation rates of the four multiplet lines are as follows:

$$\Gamma_{DQ/ZQ}^{\alpha\beta/\beta\beta} = \Gamma^a + \Gamma_{N,C'_{\alpha}}^{CSA/DD} - \Gamma_{N,NC_{\alpha}}^{CSA/DD} - \Gamma_{C',C'_{\alpha}}^{CSA/DD} + \Gamma_{C',NH^N}^{CSA/DD} - \Gamma_{C'_{\alpha},NH^N}^{DD/DD} - \Gamma_{C'_{\alpha},NC_{\alpha}}^{DD/DD} \quad (3)$$

$$\Gamma_{DQ/ZQ}^{\alpha\alpha/\beta\alpha} = \Gamma^a + \Gamma_{N,C'_{\alpha}}^{CSA/DD} + \Gamma_{N,NC_{\alpha}}^{CSA/DD} + \Gamma_{C',C'_{\alpha}}^{CSA/DD} + \Gamma_{C',NH^N}^{CSA/DD} + \Gamma_{C'_{\alpha},NH^N}^{DD/DD} + \Gamma_{C'_{\alpha},NC_{\alpha}}^{DD/DD}$$

$$\Gamma_{DQ/ZQ}^{\beta\beta/\alpha\beta} = \Gamma^a - \Gamma_{N,C'_{\alpha}}^{CSA/DD} - \Gamma_{N,NC_{\alpha}}^{CSA/DD} - \Gamma_{C',C'_{\alpha}}^{CSA/DD} - \Gamma_{C',NH^N}^{CSA/DD} + \Gamma_{C'_{\alpha},NH^N}^{DD/DD} + \Gamma_{C'_{\alpha},NC_{\alpha}}^{DD/DD}$$

where  $\Gamma^a$  is the contribution due to the autocorrelated relaxation rates and equally affects all four multiplet components,  $\Gamma_{i,kl}^{CSA/DD}$  is the CSA-dipolar cross-correlated relaxation rate for the CSA of spin  $i$  and the dipolar interaction between spins  $k$  and  $l$ , and  $\Gamma_{ij,kl}^{DD/DD}$  is the dipolar-dipolar cross-correlated relaxation rate for the two dipolar interactions between spins  $i$  and  $j$  and  $k$  and  $l$ , respectively. The notation  $\Gamma_{DQ/ZQ}^{\alpha\beta/\beta\beta}$  indicates the relaxation of the multiplet component which represents the spin state  $\alpha$  for the  $H^N$  and the spin state  $\beta$  for the  $C_{\alpha}$  in the DQ coherence and the spin state  $\beta$  for the  $H^N$  and the spin state  $\beta$  for the  $C_{\alpha}$  in the ZQ coherence, respectively. Analogously, similar notations ( $\Gamma_{DQ/ZQ}^{\alpha\alpha/\beta\alpha}$ ,  $\Gamma_{DQ/ZQ}^{\beta\alpha/\alpha\alpha}$ ,  $\Gamma_{DQ/ZQ}^{\beta\beta/\alpha\beta}$ ) describe relaxation for the other spin state combinations. As mentioned above, the two rates  $\Gamma_{C'_{\alpha},NH^N}^{DD/DD}$  and  $\Gamma_{C'_{\alpha},NC_{\alpha}}^{DD/DD}$  cannot be separated, and the sum has to be interpreted. Experimental traces for the peptide planes Gly35-Ile36, Lys27-Ala28, and Gly47-Lys48 are shown in Figure 2 for  $T = 90$  ms.

If necessary, the spectral overlap can be reduced by separation of the multiplet components corresponding to the  $\alpha$  and  $\beta$  states of the  $H^N$  spin into two subspectra,<sup>2e,5</sup> using the pulse sequence shown in Figure 3. To achieve the described separation, two experiments are acquired with  $\phi_4 = x$ ,  $\epsilon = \Delta/2$  and  $\phi_4 = y$ ,  $\epsilon = 0$ .<sup>2d</sup> The following terms are selected in separate experiments:

$$\phi_4 = x, \epsilon = \Delta/2$$

$$2C_y N_y \cos(\omega_C t_1) \cos(\pi J_{NH^N} t_1) \cos(\pi J_{C'_{\alpha}} t_1) \quad (4)$$

$$\phi_4 = y, \epsilon = 0$$

$$4C_x N_x H_z \sin(\omega_C t_1) \sin(\pi J_{NH^N} t_1) \cos(\pi J_{C'_{\alpha}} t_1)$$

Adding and subtracting the two experiments, and the associated  $F_1$  quadrature components, yields two spectra with peaks at positions  $\omega_C \pm \pi J_{C'_{\alpha}} + \pi J_{NH^N}$  (spectrum 1) and  $\omega_C \pm \pi J_{C'_{\alpha}} - \pi J_{NH^N}$  (spectrum 2). The four multiplet components present in the traces of Figure 2 can now be separated into two subspectra, both containing only two multiplet components (see Supporting Information Figure 1).

The desired rate  $\Gamma$  is obtained by linearly fitting the decay of the intensity ratios according to

$$\frac{1}{4} \ln \frac{I_1 I_2}{I_3 I_4} = \frac{1}{4} \ln \frac{I_{0,1} I_{0,2}}{I_{0,3} I_{0,4}} + \Gamma T \quad (5)$$

where  $I_{0,i}$  is the intensity  $I_i$  of the corresponding line at  $T = 0$ . The three rates  $\Gamma_{C'_{\alpha},NH^N}^{DD/DD} + \Gamma_{C'_{\alpha},NC_{\alpha}}^{DD/DD}$ ,  $\Gamma_{C',NH^N}^{CSA/DD} + \Gamma_{N,C'_{\alpha}}^{CSA/DD}$ , and  $\Gamma_{N,NC_{\alpha}}^{CSA/DD} + \Gamma_{C',C'_{\alpha}}^{CSA/DD}$  are extracted from the intensity ratios  $(1/4T) \ln \frac{I_{DQ/ZQ}^{\alpha\beta/\beta\beta} I_{DQ/ZQ}^{\beta\alpha/\alpha\alpha}}{I_{DQ/ZQ}^{\beta\beta/\alpha\beta} I_{DQ/ZQ}^{\alpha\alpha/\beta\alpha}}$  and  $(1/4T) \ln \frac{I_{DQ/ZQ}^{\alpha\alpha/\beta\alpha} I_{DQ/ZQ}^{\beta\alpha/\alpha\alpha}}{I_{DQ/ZQ}^{\beta\beta/\alpha\beta} I_{DQ/ZQ}^{\alpha\beta/\beta\beta}}$ , respectively. The rates  $\Gamma_{C'_{\alpha},NH^N}^{DD/DD} + \Gamma_{C'_{\alpha},NC_{\alpha}}^{DD/DD}$ ,  $\Gamma_{C',NH^N}^{CSA/DD} + \Gamma_{N,C'_{\alpha}}^{CSA/DD}$ , and  $\Gamma_{N,NC_{\alpha}}^{CSA/DD} + \Gamma_{C',C'_{\alpha}}^{CSA/DD}$  were measured in a 2D H(N)CO correlation with the pulse sequence shown in Figure 1 and in a 3D HNCOC correlation with the pulse sequence shown in Figure 3 for a 1.5 mM  $^2H, ^{13}C, ^{15}N$ -labeled sample of ubiquitin (VLI Research, Inc., Malvern, PA) in a  $H_2O:D_2O$  95%:5% solution at pH 4.7 and 303 K. The degree of deuteration of the nonexchangeable protons is about 95%. No effect on the measurement of the cross-correlated relaxation rates presented here is expected upon substitution of the deuterons with protons, apart from the well-known increase of autocorrelated relaxation rates of the relevant coherences. Five experiments with different constant time values were recorded (50, 70, 90, 110, and 130 ms using

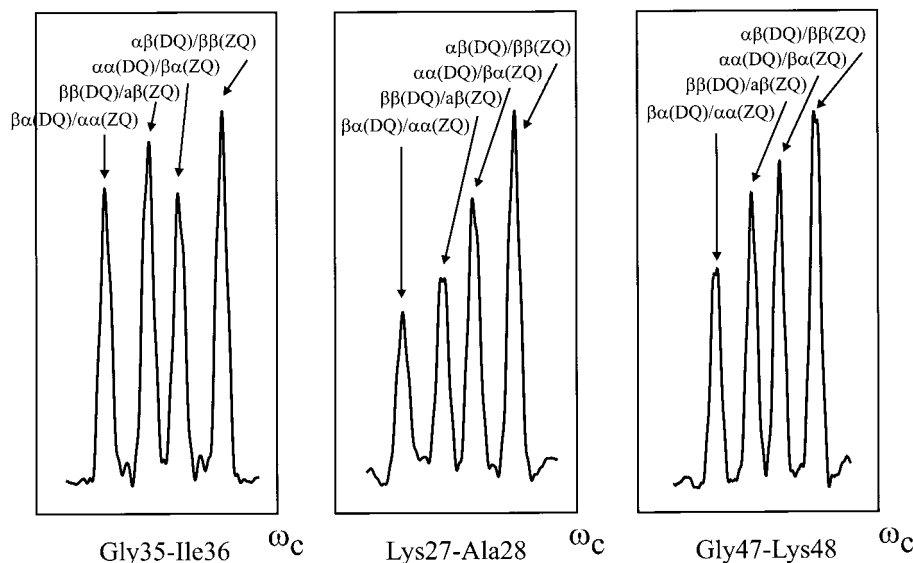


**Figure 2.** Traces in the  $\omega_1$  dimension relative to the peptide planes Gly35-Ile36, Lys27-Ala28, and Gly47-Lys48 from the experiment of Figure 1, carried out on a 1.5 mM  $^2\text{D}, ^{13}\text{C}, ^{15}\text{N}$ -labeled sample of ubiquitin in a  $\text{H}_2\text{O}:\text{D}_2\text{O}$  95:5 solution. The constant time  $T$  was 90 ms; the temperature was 303 K.

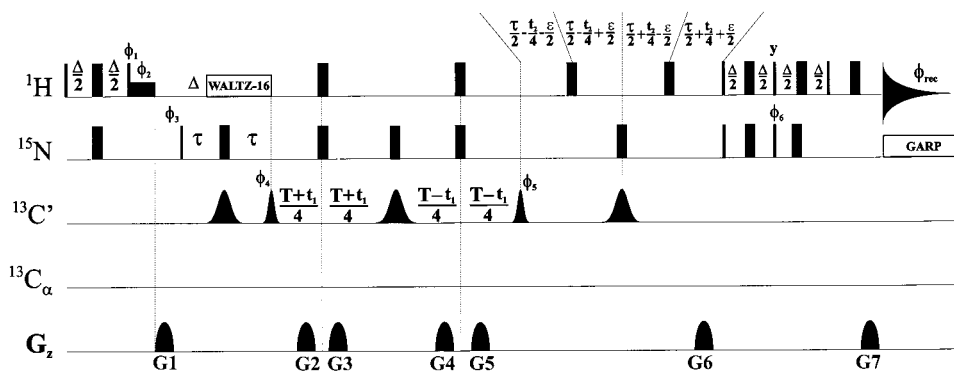


**Figure 3.** Pulse sequence for the measurement of  $\Gamma_{C'_\alpha, \text{NHN}}^{\text{DD/DD}} + \Gamma_{\text{CHN}, \text{NC}'_\alpha}^{\text{DD/DD}} + \Gamma_{\text{N}, \text{NC}'_\alpha}^{\text{CSA/DD}} + \Gamma_{C', \text{C}'_\alpha}^{\text{CSA/DD}}$ , and  $\Gamma_{C', \text{NHN}}^{\text{CSA/DD}} + \Gamma_{\text{N}, \text{CHN}}^{\text{CSA/DD}}$ . The sequence is an HNCO correlation with the following parameters values:  $\tau = 13.5$  ms;  $\Delta = 5.4$  ms;  $\phi_1 = y$ ;  $\phi_2 = -x$ ;  $\phi_3 = x, -x$ ;  $\phi_4 = 2x, 2(-x)$ ;  $\phi_6 = y$ ;  $\phi_{\text{rec}} = (x, -x, -x, x)$ ;  $\text{G2} = \text{G3} = \text{G4} = \text{G5}$ ;  $\text{G6} = (\gamma_{\text{H}}/\gamma_{\text{N}})\text{G7}$ . All phases not explicitly reported are equal to  $x$ . Separation of the lines corresponding to the  $\alpha$  and  $\beta$  states of the  $\text{H}^{\text{N}}$  spin in two subspectra is achieved by adding and subtracting two experiments acquired with  $\epsilon = \Delta/2$ ,  $\phi_4 = x$  and  $\epsilon = 0$ ,  $\phi_4 = y$ , as explained in the text. Quadrature detection is achieved in  $t_1$  by States-TPPI on  $\phi_4$ , and in  $t_2$  by adding and subtracting two fids acquired with  $\phi_6 = y$ ,  $\text{G6} = A$  and  $\phi_6 = -y$ ,  $\text{G6} = -A$ , respectively.  $^{13}\text{C}$  spins are irradiated with selective pulses ( $\text{G4}(90^\circ) = 512 \mu\text{s}$ ;  $\text{Q3}(180^\circ) = 768 \mu\text{s}$ ). The field strength for proton decoupling is 4.1 kHz for nitrogen decoupling during acquisition 1.0 kHz. The proton carrier is on water. The pulse with phase  $\phi_2$  is a low-power selective  $\pi/2$  pulse of duration 2 ms. Five 3D experiments with different constant time values have been acquired ( $T = 70, 80, 90, 100,$  and  $110$  ms), yielding a total measurement time of 5 days and resulting in  $128(t_1) \times 16(t_2) \times 1024(t_3)$  complex points for each experiment. The final size of the matrix was  $512(\omega_1) \times 32(\omega_2) \times 2048(\omega_3)$  after linear prediction in  $\omega_1$  and zero-filling in all three dimensions.

the experiment shown in Figure 1 and 70, 80, 90, 100, and 110 ms for the experiment shown in Figure 3).

## Results

**NMR Data.** The proposed pulse sequences shown in Figures 1 and 3, described in detail in the Methods section, have been used to derive  $\Gamma_{C'_\alpha, \text{NHN}}^{\text{DD/DD}} + \Gamma_{\text{CHN}, \text{NC}'_\alpha}^{\text{DD/DD}}$ ,  $\Gamma_{C', \text{NHN}}^{\text{CSA/DD}} + \Gamma_{\text{N}, \text{CHN}}^{\text{CSA/DD}}$ , and  $\Gamma_{\text{N}, \text{NC}'_\alpha}^{\text{CSA/DD}} + \Gamma_{C', \text{C}'_\alpha}^{\text{CSA/DD}}$  from the analysis of multiplet lines. Representative traces are shown in Figure 2 for the pulse sequences of Figure 1. An excellent resolution of the multiplet components is obtained. The fitting of the experimental data to eq 5 is rather good despite the small size of the corresponding rates. Estimated errors of the measured rates were derived from signal-to-noise values according to the standard error propagation analysis. These errors correlate quite well with the standard errors derived from the fitting of the five data points to eq 5.

The three cross-correlated relaxation rates  $\Gamma_{C'_\alpha, \text{NHN}}^{\text{DD/DD}} + \Gamma_{\text{CHN}, \text{NC}'_\alpha}^{\text{DD/DD}}$ ,  $\Gamma_{C', \text{NHN}}^{\text{CSA/DD}} + \Gamma_{\text{N}, \text{CHN}}^{\text{CSA/DD}}$ , and  $\Gamma_{\text{N}, \text{NC}'_\alpha}^{\text{CSA/DD}} + \Gamma_{C', \text{C}'_\alpha}^{\text{CSA/DD}}$ , derived

from the experiment shown in Figure 3, are reported in Figure 4 as a function of the polypeptide sequence. The experimental  $\Gamma_{C'_\alpha, \text{NHN}}^{\text{DD/DD}} + \Gamma_{\text{CHN}, \text{NC}'_\alpha}^{\text{DD/DD}}$  rate (Figure 4a) significantly deviates from the expected  $-0.097$  Hz value for a peptide plane in standard geometry<sup>3</sup> in the absence of motion. The nonuniform deviation from the static value indicates the presence of anisotropic motions, in agreement with previous studies.<sup>2f-1</sup> The mean value of the  $\Gamma_{C'_\alpha, \text{NHN}}^{\text{DD/DD}} + \Gamma_{\text{CHN}, \text{NC}'_\alpha}^{\text{DD/DD}}$  rates along the polypeptide chain is  $-0.12$  Hz. Although the average error is large ( $\sim 0.16$  Hz) with respect to the absolute values, the standard deviation of the rates of the different peptide planes from the mean value ( $-0.12$  Hz) is 0.22 Hz, which provides evidence that the change in the determined cross-correlated relaxation rates along the polypeptide chain is significant. As mentioned before, for a small protein like ubiquitin (MW 7 kDa), the  $\Gamma_{C'_\alpha, \text{NHN}}^{\text{DD/DD}} + \Gamma_{\text{CHN}, \text{NC}'_\alpha}^{\text{DD/DD}}$  rate could be measured at a low degree of accuracy in the employed measurement time of 5 days. The

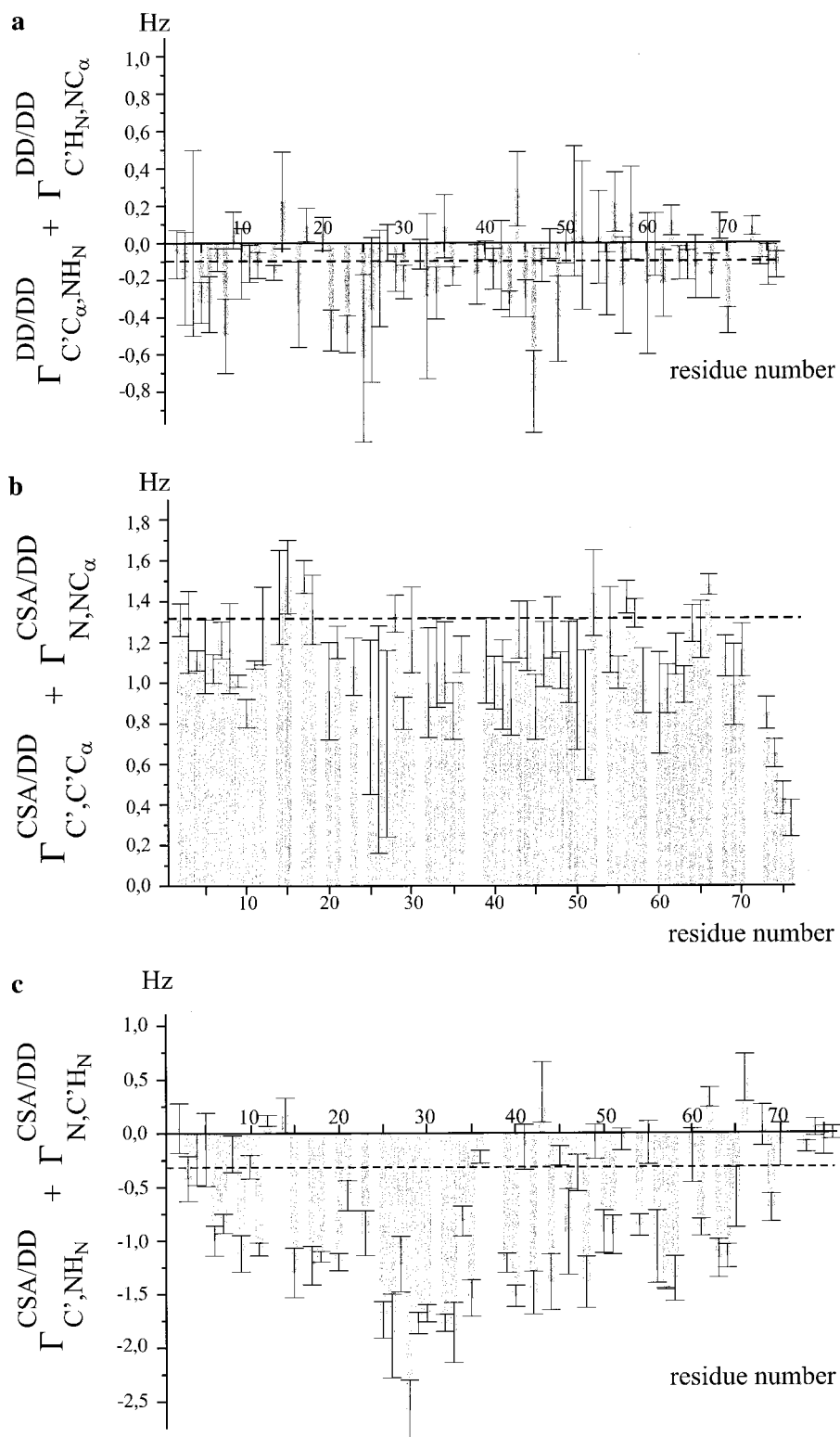


**Figure 4.** Experimental values for the three rates  $\Gamma_{C',\alpha,NHN}^{DD/DD} + \Gamma_{C'HN,NC\alpha}^{DD/DD}$  (a),  $\Gamma_{N,NC\alpha}^{CSA/DD} + \Gamma_{C',C'\alpha}^{CSA/DD}$  (b), and  $\Gamma_{C',NHN}^{CSA/DD} + \Gamma_{N,C'HN}^{CSA/DD}$  (c). The rates are represented by gray bars; the errors are in black. The dashed lines represent the values of the rates in the absence of motion assuming standard geometry of the peptide plane.

error bars of Figure 4a represent standard errors, corresponding to a 68% confidence interval. An error range twice as large, which corresponds to a 90% confidence interval, would allow the calculated value of  $-0.097$  Hz for the  $\Gamma_{C',\alpha,NHN}^{DD/DD} + \Gamma_{C'HN,NC\alpha}^{DD/DD}$  rate in the absence of motion for most of the peptide planes. Unfortunately, the values of the  $\Gamma_{C',\alpha,NHN}^{DD/DD} + \Gamma_{C'HN,NC\alpha}^{DD/DD}$  rates summarized in Figure 4a are too inaccurate for a rigorous

quantitative analysis. Thus, these values will be used in the following only as an indication of the most probable direction of deviation of the rates upon internal motions from the calculated value of  $-0.097$  Hz. The average values for the rates  $\Gamma_{N,NC\alpha}^{CSA/DD} + \Gamma_{C',C'\alpha}^{CSA/DD}$  and  $\Gamma_{C',NHN}^{CSA/DD} + \Gamma_{N,C'HN}^{CSA/DD}$  are  $1.08 \pm 0.15$  and  $-0.76 \pm 0.16$  Hz with standard deviations from the corresponding average value of 0.24 and 0.69 Hz, respectively. Changes

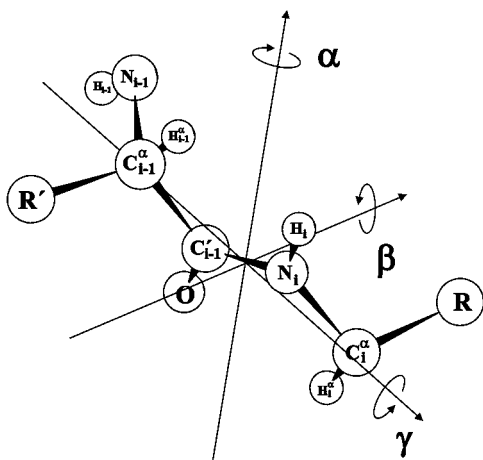


**Figure 5.** Schematic representation of the axes of the GAF model of motion with respect to the peptide plane.

of the three measured rates along the polypeptide chain indicate anisotropic reorientations of the peptide planes and/or possible variations of the carbonyl and nitrogen CSA tensors depending on secondary structure and hydrogen bonding.

### Data Analysis

We applied the Gaussian axial fluctuation (GAF) model<sup>4</sup> to interpret the three cross-correlated relaxation rates measured for ubiquitin in terms of internal reorientation of the peptide planes. In this model, fluctuations of the peptide plane around three perpendicular axes are assumed with Gaussian distributions of the respective amplitudes of motion (Figure 5). The model was developed from molecular dynamics (MD) simulation carried out on the peptide antamanide and on the protein ubiquitin.<sup>4</sup> In these MD simulations, motions with the largest amplitude were found around the  $\gamma$  axis, which connects the  $C_{\alpha,i-1}$  and  $C_{\alpha,i}$  nuclei, forming an angle of about  $40^\circ$  with the peptide bond. The  $\alpha$  axis is perpendicular to the  $\gamma$  axis, and both axes lie in the peptide plane, while the  $\beta$  axis is perpendicular to the peptide plane (Figure 5). In MD simulations the amplitudes of motion around the  $\alpha$  and  $\beta$  axes,  $\sigma_\alpha$  and  $\sigma_\beta$ , were found to be similar. The relative variation of the two pairs of rates  $\Gamma_{C'_{\alpha},NH_N}^{DD/DD} + \Gamma_{C'_{HN},NC_\alpha}^{DD/DD}$ ,  $\Gamma_{N,N,C_\alpha}^{CSA/DD} + \Gamma_{C',C'_\alpha}^{CSA/DD}$ , and  $\Gamma_{C',NH_N}^{CSA/DD} + \Gamma_{N,C'_{HN}}^{CSA/DD}$ , upon motions around  $\alpha$ ,  $\beta$ , and  $\gamma$ , calculated according to the GAF model in the range between  $0^\circ$  and  $30^\circ$ , are shown in Figure 6. Details of the parameters used in the theoretical calculations are given in the figure caption. The values for the carbonyl CSA tensors were  $(\sigma_{11} - \sigma_{33}) = -153$  ppm and  $(\sigma_{22} - \sigma_{33}) = -85$  ppm, and  $\alpha_C$ , representing the angle between the  $\sigma_{11}$  component and the peptide bond, was  $41^\circ$ , as derived from an average of several solid-state NMR studies.<sup>6</sup> The rate  $\Gamma_{C'_{\alpha},NH_N}^{DD/DD} + \Gamma_{C'_{HN},NC_\alpha}^{DD/DD}$  shows major changes for motions around all the axes  $\alpha$ ,  $\beta$ , and  $\gamma$ . The rate  $\Gamma_{C',NH_N}^{CSA/DD} + \Gamma_{N,C'_{HN}}^{CSA/DD}$  is very insensitive to  $\alpha$ -motions, while the rate  $\Gamma_{N,N,C_\alpha}^{CSA/DD} + \Gamma_{C',C'_\alpha}^{CSA/DD}$  changes dramatically upon reorientations around the  $\alpha$  axis. Since the various rates behave differently in the presence of fluctuations around the three axes, the amplitude and phase of motions can be defined accurately by a combined set of different cross-correlated relaxation rates. In the GAF motional regime, assuming that the amplitude of motions around  $\alpha$  and  $\beta$ ,  $\sigma_\alpha$  and  $\sigma_\beta$ , are equal and that  $\sigma_\alpha$ ,  $\sigma_\beta$ , and  $\sigma_\gamma$  vary between  $0^\circ$  and

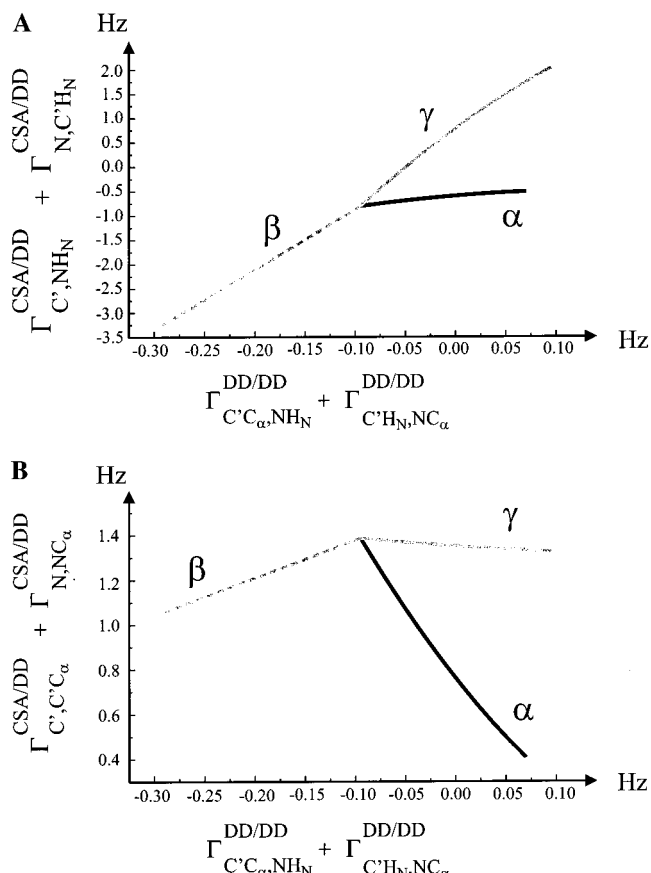


**Figure 6.** Relative variation of rates  $(\Gamma_{C',NH_N}^{CSA/DD} + \Gamma_{N,C'_{HN}}^{CSA/DD}) / (\Gamma_{C',NH_N}^{DD/DD} + \Gamma_{C'_{HN},NC_\alpha}^{DD/DD})$  in panel A and  $(\Gamma_{N,N,C_\alpha}^{CSA/DD} + \Gamma_{C',C'_\alpha}^{CSA/DD}) / (\Gamma_{C',C'_\alpha}^{CSA/DD} + \Gamma_{N,N,C_\alpha}^{CSA/DD})$  in panel B) upon motion around a single axis of the GAF model. Motions around the  $\beta$  axis are represented by a black continuous line, those around the  $\alpha$  axis by a gray dashed line, and those around the  $\gamma$  axis by a gray continuous line. The maximum  $\sigma$  of the Gaussian distribution of amplitude of motions is  $30^\circ$ . The parameters used in the calculation are as follows:  $^{13}C'$  CSA tensor,  $(\sigma_{11} - \sigma_{33}) = -153$  ppm,  $(\sigma_{22} - \sigma_{33}) = -85$  ppm,  $\alpha_C$  (angle between the component  $\sigma_{11}$  and the peptide bond) =  $41^\circ$ ;  $^{15}N$  CSA tensor, axially symmetric,  $\Delta\sigma_N = -170$  ppm,  $\alpha_N$  (angle between the axis of symmetry and the  $NH_N$  bond) =  $19^\circ$ ;  $\tau_c = 4.1$  ns and  $\tau_1 = 10$  ps;  $r_{NH_N} = 1.04$  Å;  $r_{C'_\alpha} = 1.52$  Å;  $r_{C'_{HN}} = 2.02$  Å;  $r_{C'_N} = 1.33$  Å;  $r_{NC_\alpha} = 2.40$  Å.

$30^\circ$ , the rate  $\Gamma_{C'_{\alpha},NH_N}^{DD/DD} + \Gamma_{C'_{HN},NC_\alpha}^{DD/DD}$  ranges from 0.09 to  $-0.11$  Hz, the rate  $\Gamma_{C',NH_N}^{CSA/DD} + \Gamma_{N,C'_{HN}}^{CSA/DD}$  from 1.91 to  $-1.98$  Hz, and the rate  $\Gamma_{N,N,C_\alpha}^{CSA/DD} + \Gamma_{C',C'_\alpha}^{CSA/DD}$  from 1.39 to 0.28 Hz. For several peptide planes the  $\Gamma_{C'_{\alpha},NH_N}^{DD/DD} + \Gamma_{C'_{HN},NC_\alpha}^{DD/DD}$  rate falls outside this range (for example, planes 20–21, 22–23, and 45–46 in Figure 4a). In contrast, the measured values for the other two rates are consistently within the calculated range.

Out of the 75 available peptide planes, 55 have been analyzed with the GAF model of motion (Table 3). The C-terminal residues 71–76 were not considered in the analysis due to the high degree of conformational disorder. Residues 19, 37, and 38 are prolines, and no NMR data are available for the corresponding planes. Data on planes 12–13, 15–16, 21–22, 23–24, 30–31, 52–53, 58–59, and 66–67 are missing because of spectral overlap or low signal-to-noise. For planes 20–21, 22–23, and 45–46 the observed  $\Gamma_{C'_{\alpha},NH_N}^{DD/DD} + \Gamma_{C'_{HN},NC_\alpha}^{DD/DD}$  rates lie outside of the calculated range. Imposing  $\sigma_\alpha = \sigma_\beta$  greatly limits the possible range of the rate  $\Gamma_{C'_{\alpha},NH_N}^{DD/DD} + \Gamma_{C'_{HN},NC_\alpha}^{DD/DD}$ , because motions around the two axes have opposite effects on that rate

(6) (a) Teng, Q.; Iqbal, M.; Cross, T. A. *J. Am. Chem. Soc.* **1992**, *114*, 5312–5321. (b) Oas, T. G.; Hartzell, C. J.; McMahon, T. J.; Drobny, G. P.; Dahlquist, F. W. *J. Am. Chem. Soc.* **1987**, *109*, 5956–5962.

**Table 3.** Summary of the Peptide Planes of the Protein Ubiquitin Whose Relaxation Data Were Considered in the Dynamic Analysis

12–13, 15–16, 21–22, 23–24, 30–31, 52–53, 58–59, 66–67	relaxation data not available
71–76	high conformational flexibility
20–21, 22–23, 45–46	excluded from the analysis due to too large $\Gamma_{C'_\alpha, \text{NHN}}^{\text{DD/DD}} + \Gamma_{C'_{\text{HN}}, \text{NC}_\alpha}^{\text{DD/DD}}$ rate
18–19, 36–37, 37–38	relaxation data not available (Pro19, Pro37, Pro38)
1–2, 2–3, 3–4, 10–11, 11–12, 33–34, 38–39, 40–41, 41–42, 46–47, 47–48, 49–50, 50–51, 51–52, 53–54, 54–55, 57–58, 59–60, 60–61, 61–62, 63–64, 64–65, 67–68	relaxation data explainable with the restricted GAF model
24–25, 25–26, 26–27, 27–28, 28–29, 29–30, 31–32, 32–33	relaxation data explainable with the extended GAF model
4–5, 5–6, 6–7, 7–8, 8–9, 9–10, 13–14, 14–15, 16–17, 17–18, 19–20, 34–35, 35–36, 39–40, 42–43, 43–44, 44–45, 55–56, 62–63, 68–69, 69–70, 70–71	relaxation data not explainable with the GAF model

(Figure 6). In an extended GAF model ( $\sigma_\alpha \neq \sigma_\beta \neq \sigma_\gamma$ ),  $\Gamma_{C'_\alpha, \text{NHN}}^{\text{DD/DD}} + \Gamma_{C'_{\text{HN}}, \text{NC}_\alpha}^{\text{DD/DD}}$  ranges from  $-0.3$  to  $-0.1$  Hz. However, the values of the  $\Gamma_{C'_\alpha, \text{NHN}}^{\text{DD/DD}} + \Gamma_{C'_{\text{HN}}, \text{NC}_\alpha}^{\text{DD/DD}}$  rate for planes 20–21, 22–23, and 45–46 are still outside the accessible range, even in this extended GAF model. For plane 22–23, slow internal motion is observed in MD simulations.<sup>1c</sup> All three planes were not included in further analysis. All in all, the number of peptide planes that could be analyzed was reduced by 20 to 55.

## Discussion

Of the remaining 55 sets of cross-correlated relaxation rates, 33 could be fitted to the GAF model of motion (Table 3): the values of  $\sigma_\alpha$ ,  $\sigma_\beta$ , and  $\sigma_\gamma$  which best fit the measured parameters are reported in Table 4.

Twenty-five peptide planes show motions which can be described with the restricted GAF model, implying  $\sigma_\alpha = \sigma_\beta \neq \sigma_\gamma$ .

Eight peptide planes require an extended GAF model with  $\sigma_\alpha \neq \sigma_\beta \neq \sigma_\gamma$ . These planes are all located in the long  $\alpha$ -helix which spans from residue 23 to residue 34 (Table 3). All residues in this helix exhibit extraordinarily large and negative  $\Gamma_{C'_{\text{NHN}}, \text{NC}_\alpha}^{\text{CSA/DD}} + \Gamma_{C'_{\text{HN}}, \text{NC}_\alpha}^{\text{CSA/DD}}$  rates, relatively low  $\Gamma_{N, \text{NC}_\alpha}^{\text{CSA/DD}} + \Gamma_{C', \text{C}'_\alpha}^{\text{CSA/DD}}$  rates, and negative  $\Gamma_{C'_\alpha, \text{NHN}}^{\text{DD/DD}} + \Gamma_{C'_{\text{HN}}, \text{NC}_\alpha}^{\text{DD/DD}}$  rates. All residues belonging to the helix have a  $z$ -score value more negative than  $-1.5$  for  $\Gamma_{C'_{\text{NHN}}, \text{NC}_\alpha}^{\text{CSA/DD}} + \Gamma_{C'_{\text{HN}}, \text{NC}_\alpha}^{\text{CSA/DD}}$ , while for  $\Gamma_{N, \text{NC}_\alpha}^{\text{CSA/DD}} + \Gamma_{C', \text{C}'_\alpha}^{\text{CSA/DD}}$  and  $\Gamma_{C'_\alpha, \text{NHN}}^{\text{DD/DD}} + \Gamma_{C'_{\text{HN}}, \text{NC}_\alpha}^{\text{DD/DD}}$  the  $z$ -score value exceeds  $-1.5$  only for the central helical residues (25–29). The deviation of the three rates from their average values is statistically significant, in particular for  $\Gamma_{C'_{\text{NHN}}, \text{NC}_\alpha}^{\text{CSA/DD}} + \Gamma_{C'_{\text{HN}}, \text{NC}_\alpha}^{\text{CSA/DD}}$ , and all the three rates qualitatively point to the presence of large  $\beta$ -motions and moderate  $\alpha/\gamma$ -motions (Figure 6).

Interestingly, most of the peptide planes whose rates cannot be interpreted in terms of the GAF model are situated in  $\beta$ -sheet regions (plane 13–14 to plane 16–17; plane 42–43 to plane 44–45; plane 48–49; planes 65–66, 68–69, and 69–70). The remaining 11 planes belong either to turns or to unstructured regions.

Recently, autocorrelated nitrogen and carbonyl  $T_1$  and  $T_2$  data for ubiquitin were interpreted in terms of GAF-type internal motions and compared with MD results.<sup>1c</sup> For the 24 peptide planes not within  $\alpha$ -helix 23–34, our results are in quite good agreement with this previous study<sup>1c</sup> with respect to the overall amplitude of motions, but they differ significantly in the distribution of the motion among the three axes. Our analysis revealed several cases where  $\sigma_{\alpha/\beta}$  is larger than  $\sigma_\gamma$  (planes 5–6, 6–7, 10–11, 38–39, 41–42, 48–49, 49–50, 50–51, 53–54, 57–58, and 60–61), which is in disagreement with MD simulations and with the mentioned analysis of autocorrelated

**Table 4.** Values of  $\sigma_\alpha$ ,  $\sigma_\beta$ , and  $\sigma_\gamma$  Resulting from the Fitting of the Three  $\Gamma_{C'_\alpha, \text{NHN}}^{\text{DD/DD}} + \Gamma_{C'_{\text{HN}}, \text{NC}_\alpha}^{\text{DD/DD}}$ ,  $\Gamma_{C'_{\text{NHN}}, \text{NC}_\alpha}^{\text{CSA/DD}} + \Gamma_{N, \text{NC}_\alpha}^{\text{CSA/DD}}$ , and  $\Gamma_{N, \text{NC}_\alpha}^{\text{CSA/DD}} + \Gamma_{C', \text{C}'_\alpha}^{\text{CSA/DD}}$  Cross-Correlated Relaxation Rates to a GAF Model of Motion

residue number (secondary structure)	$\sigma_\alpha$	$\sigma_\beta$	$\sigma_\gamma$
2 ( $\beta$ -sheet)	4	4	14
3 ( $\beta$ -sheet)	6	6	10
4 ( $\beta$ -sheet)	10	10	14
6 ( $\beta$ -sheet)	12	12	8
7 ( $\beta$ -sheet)	8	8	6
11 (coil)	12	12	8
12 ( $\beta$ -sheet)	0	0	14
25 ( $\alpha$ -helix)	0	26	14
26 ( $\alpha$ -helix)	0	28	14
27 ( $\alpha$ -helix)	0	26	20
28 ( $\alpha$ -helix)	0	18	6
29 ( $\alpha$ -helix)	0	30	20
30 ( $\alpha$ -helix)	0	18	8
32 ( $\alpha$ -helix)	0	26	16
33 ( $\alpha$ -helix)	0	24	6
34 ( $\alpha$ -helix)	0	18	16
39 ( $\alpha$ -helix)	12	12	2
41 ( $\beta$ -sheet)	14	14	18
42 ( $\beta$ -sheet)	16	16	2
47 (bend)	8	8	12
48 ( $\beta$ -sheet)	12	12	2
50 (coil)	14	14	10
51 (turn)	16	16	12
52 (bend)	0	0	12
54 (bend)	8	8	6
55 (bridge)	12	12	16
58 ( $\alpha$ -helix)	14	14	2
60 (coil)	16	16	18
61 (coil)	12	12	10
62 (turn)	8	8	18
64 (bend)	8	8	0
65 (coil)	6	6	8
68 ( $\beta$ -sheet)	10	10	16

<sup>a</sup> The rates of most of the residues in  $\beta$ -sheet regions cannot be fitted to the GAF model of motion using the parameters of Figure 6. The peptide planes in  $\alpha$ -helix 23–34 show no  $\alpha$ -motion, high  $\beta$ -motion, and medium-range  $\gamma$ -motion.

data.<sup>1c</sup> This discrepancy could be explained either by the higher sensitivity of cross-correlated relaxation data to the anisotropy of motion as compared to autocorrelated data or by variations of the carbonyl CSA tensor along the polypeptide chain, which would affect the interpretation of both autocorrelated and cross-correlated data.

The  $\alpha$ -helix 23–34 shows a very peculiar behavior. Eight of the nine peptide planes for which cross-correlated relaxation data are available cannot be fitted with a restricted GAF model ( $\sigma_\alpha = \sigma_\beta$ ). This is true for both the  $\Gamma_{C'_{\text{NHN}}, \text{NC}_\alpha}^{\text{CSA/DD}} + \Gamma_{N, \text{NC}_\alpha}^{\text{CSA/DD}}$  and  $\Gamma_{N, \text{NC}_\alpha}^{\text{CSA/DD}} + \Gamma_{C', \text{C}'_\alpha}^{\text{CSA/DD}}$  rates and for the complete set of the three measured rates. The results for the fitting of the cross-correlated relaxation data of all peptide planes belonging to the  $\alpha$ -helix to

an extended GAF model ( $\sigma_\alpha \neq \sigma_\beta \neq \sigma_\gamma$ ) are shown in Table 4. All residues show large motions around the axis  $\beta$  combined with moderate  $\gamma$ -motion, with  $\sigma_\beta$  being almost 2 times as large as  $\sigma_\gamma$ . This characteristic motion is found in the extended GAF model for every residue belonging to the  $\alpha$ -helix (Table 4). We have investigated two potential reasons for the large deviations of these results from what is found in MD simulations ( $\sigma_\alpha = \sigma_\beta < \sigma_\gamma$ ): (a) systematic deviation of carbonyl CSA values from the used ones<sup>6</sup> and (b) the presence of cooperative motions of all the residues belonging to the  $\alpha$ -helix on a time scale similar to the overall correlation time. A rotation of the direction of the carbonyl CSA principal axis  $\sigma_{11}$  of  $10^\circ$  around the  $\sigma_{33}$  axis ( $\alpha_C = 51^\circ$ ) causes an increase in the absolute value of the rates  $\Gamma_{C',NHN}^{CSA/DD} + \Gamma_{N,C'HN}^{CSA/DD}$  and  $\Gamma_{N,NC_\alpha}^{CSA/DD} + \Gamma_{C',C'_\alpha}^{CSA/DD}$  in the absence of motion of 100% and 10%, respectively ( $\Gamma_{C',NHN}^{CSA/DD} + \Gamma_{N,C'HN}^{CSA/DD}$  changes from  $-0.80$  to  $-1.64$  Hz and  $\Gamma_{N,NC_\alpha}^{CSA/DD} + \Gamma_{C',C'_\alpha}^{CSA/DD}$  from  $1.38$  to  $1.55$  Hz for a  $\tau_c$  of  $4.1$  ns). Assuming such a change in the CSA principal axes direction, the CSA-dipolar cross-correlated relaxation rates could be interpreted with  $\beta$ -motions of significantly less amplitude, because  $\Gamma_{C',NHN}^{CSA/DD} + \Gamma_{N,C'HN}^{CSA/DD}$  would already be large and negative ( $-1.6$  Hz) in the absence of motion.  $\Gamma_{N,NC_\alpha}^{CSA/DD} + \Gamma_{C',C'_\alpha}^{CSA/DD}$  is less affected than  $\Gamma_{C',NHN}^{CSA/DD} + \Gamma_{N,C'HN}^{CSA/DD}$  by this change in the carbonyl CSA principal axes direction. To explain the low values of  $\Gamma_{N,NC_\alpha}^{CSA/DD} + \Gamma_{C',C'_\alpha}^{CSA/DD}$ , a certain degree of motion must be assumed:  $\Gamma_{N,NC_\alpha}^{CSA/DD} + \Gamma_{C',C'_\alpha}^{CSA/DD}$  diminishes upon motions around all three axes, and its value alone cannot give unambiguous information on the anisotropy of the internal reorientations. The amplitude of motion around the  $\alpha$  axis is particularly undetermined, as  $\Gamma_{C',NHN}^{CSA/DD} + \Gamma_{N,C'HN}^{CSA/DD}$  remains almost constant upon this kind of motion. If only the two  $\Gamma_{C',NHN}^{CSA/DD} + \Gamma_{N,C'HN}^{CSA/DD}$  and  $\Gamma_{N,NC_\alpha}^{CSA/DD} + \Gamma_{C',C'_\alpha}^{CSA/DD}$  rates are considered, the peculiar behavior of the helix could be associated with a systematic deviation of the direction of the CSA tensor with respect to the commonly used one<sup>6</sup> and small-amplitude  $\alpha$ - and  $\beta$ - motions, possibly with  $\sigma_\alpha = \sigma_\beta$ . The value of the rate  $\Gamma_{C'_\alpha,NHN}^{DD/DD} + \Gamma_{C'HN,NC_\alpha}^{DD/DD}$ , which is not affected by uncertainties of the CSA tensor, is decisive in distinguishing the direction of the motion (Figure 6). If  $\Gamma_{C'_\alpha,NHN}^{DD/DD} + \Gamma_{C'HN,NC_\alpha}^{DD/DD}$  is negative,  $\beta$ -motions must be present, either accompanied or not by  $\alpha$ - and  $\gamma$ -motions of smaller amplitude, depending on the absolute value of the rate. If the rate is positive,  $\alpha$ - and  $\gamma$ -motions are dominant. This case is a typical example where the analysis of more than one cross-correlated relaxation rate at the same time is necessary to distinguish local structural variability from dynamics and to define the direction of motion. In  $\alpha$ -helix 23–34, the values for the  $\Gamma_{C'_\alpha,NHN}^{DD/DD} + \Gamma_{C'HN,NC_\alpha}^{DD/DD}$  rate are predominantly negative or close to zero. The values of this rate are independent of any assumption on the CSA tensor and are in agreement with considerable  $\beta$ -motions accompanied by either  $\alpha$ - or  $\gamma$ -motions of smaller amplitude. Although the values of the  $\Gamma_{C'_\alpha,NHN}^{DD/DD} + \Gamma_{C'HN,NC_\alpha}^{DD/DD}$  rates are rather inaccurate, they indicate a clear tendency of the residues of the helix to assume most probably negative values, which rules out the possibility of  $\sigma_\gamma > \sigma_\beta, \sigma_\alpha$ , as observed in MD simulations. The present level of accuracy of the  $\Gamma_{C'_\alpha,NHN}^{DD/DD} + \Gamma_{C'HN,NC_\alpha}^{DD/DD}$  rates does not allow us to distinguish between the interpretation assuming no deviation of the CSA principal axis values and direction from the standard ones,<sup>6</sup> which includes large  $\beta$ -motions accompanied by  $\gamma$ -motions of smaller amplitude (Table 4), and the interpreta-

tion assuming a deviation of the principal axis direction of the carbonyl CSA away from the peptide bond (small-amplitude  $\alpha$ - and  $\beta$ -motions). In principle, this distinction would be possible if the  $\Gamma_{C'_\alpha,NHN}^{DD/DD} + \Gamma_{C'HN,NC_\alpha}^{DD/DD}$  rate could be measured with high accuracy, as is likely to be the case for larger proteins. If the cross-correlated relaxation data are interpreted assuming no deviation of the CSA parameters from the values extracted from solid-state data, we observed that an extended GAF model can fit the experimental data in the helix assuming large  $\beta$ - and  $\gamma$ -motions of comparable amplitudes for each residue. This might indicate the presence of cooperative motion on a slow time scale. Such cooperative motions, which were already observed by others for  $\alpha$ -helices,<sup>9</sup> would not be detectable in MD simulations because of either limited simulation time or inappropriate force field. The extended GAF model reveals no motion around the  $\alpha$  axis. This axis is almost parallel to the NH vectors, and it has almost the same orientation as the helix axis. Angular fluctuations around axes perpendicular to  $\alpha$  are compatible with a reorientation of the helix axis itself. Anyway, this motion cannot be described by angular reorientations around two perpendicular axes with Gaussian distribution of amplitudes, and a more complicated motional model needs to be developed.

Most of the 23 data sets which could not be fitted to a GAF model are located in  $\beta$ -sheet regions. This finding is in good agreement with results of a recent study on the  $\Gamma_{C',NHN}^{CSA/DD}$  rate,<sup>2h</sup> where extreme values of the rate have been found in the  $\beta$ -sheet region. The incompatibility with the GAF model is already evident from a reduced set of data comprising  $\Gamma_{C',NHN}^{CSA/DD} + \Gamma_{N,C'HN}^{CSA/DD}$  and  $\Gamma_{C'_\alpha,NHN}^{DD/DD} + \Gamma_{C'HN,NC_\alpha}^{DD/DD}$ . No obvious trends are observed in the measured rates, as was the case for the  $\alpha$ -helix. This observation potentially reflects considerable deviations of carbonyl CSA principal axis values and directions from the ones extracted from solid-state data.<sup>6</sup> The interpretation of cross-correlated relaxation rates by fitting the experimental data to both motional parameters and carbonyl and nitrogen CSA principal axis values and directions would be the method of choice in order to overcome the problem. However, this approach requires the analysis of an extended set of relaxation rates, including autocorrelated ones, and is pursued in our and in other laboratories.<sup>2h</sup>

The peptide plane 27–28 gives an example of the large effect that changes in CSA values can have on motional parameters and of the importance of a combined analysis of several rates, which are influenced by directions of motion in a different manner. This plane exhibits a very large and negative  $\Gamma_{C',NHN}^{CSA/DD} + \Gamma_{N,C'HN}^{CSA/DD}$  rate, which points to the presence of large  $\beta$ -motions. On the other hand, the  $\Gamma_{C'_\alpha,NHN}^{DD/DD} + \Gamma_{C'HN,NC_\alpha}^{DD/DD}$  rate cannot be smaller than  $-0.1$  Hz, which is incompatible with large reorientation around the  $\beta$  axis. Additional large  $\alpha$ -motion would explain the values of these two rates because  $\alpha$ -motions do not have a big effect on the  $\Gamma_{C',NHN}^{CSA/DD} + \Gamma_{N,C'HN}^{CSA/DD}$  rate but can compensate the negative trend of the  $\Gamma_{C'_\alpha,NHN}^{DD/DD} + \Gamma_{C'HN,NC_\alpha}^{DD/DD}$  rate upon motions around the  $\beta$  axis. Large  $\alpha$ - and  $\beta$ -motions, however, produce extremely low  $\Gamma_{N,NC_\alpha}^{CSA/DD} + \Gamma_{C',C'CN}^{CSA/DD}$  rates, while the 27–28 peptide plane shows a relatively high value for this rate. The only way of interpreting this combined set of

(7) Vijay-Kumar, S.; Bugg, C. E.; Cook, W. J. *J. Mol. Biol.* **1997**, *194*, 531–544.

(8) Sitkoff, D.; Case, D. A. *Prog. Nucl. Magn. Reson. Spectrosc.* **1998**, *32*, 165–190.

(9) Fischer, M. W. F.; Zeng, L.; Pang, Y.; Majumdar, A.; Zuiderweg, E. R. P. *Proc. Natl. Acad. Sci. U.S.A.* **1998**, *95*, 8016–8019.

rates in terms of the GAF model is to assume changes in the directions of the CSA principal axes of the carbonyl nucleus. The required change is a rotation of  $15^\circ$  around the  $\sigma_{33}$  axis. With this assumption, the rates are compatible with the GAF model. The required changes in the carbonyl CSA axis directions is justified by the fact that the carbonyl of Lys27 bears two hydrogen bonds, with the NH of Gln31 and the side chain of Gln41 as donors, according to the high-resolution X-ray structure of ubiquitin.<sup>7</sup> Quantum mechanical calculations<sup>8</sup> revealed that hydrogen bonds can substantially influence CSA values, which necessitates the fitting of CSA parameters together with motional parameters to an extended set of relaxation data.

## Conclusions

We have presented a combined analysis of fast internal motions of the protein ubiquitin by means of the three cross-correlated relaxation rates,  $\Gamma_{C'_\alpha, \text{NH}^N}^{\text{DD/DD}} + \Gamma_{C'^\text{H}^N, \text{NC}_\alpha}^{\text{DD/DD}}$ ,  $\Gamma_{C', \text{NH}^N}^{\text{CSA/DD}} + \Gamma_{N, C'^\text{H}^N}^{\text{CSA/DD}}$ , and  $\Gamma_{N, \text{NC}_\alpha}^{\text{CSA/DD}} + \Gamma_{C', C'_\alpha}^{\text{CSA/DD}}$ . A new pulse sequence has been proposed to measure the three parameters in a single experiment. The  $\Gamma_{C'_\alpha, \text{NH}^N}^{\text{DD/DD}} + \Gamma_{C'^\text{H}^N, \text{NC}_\alpha}^{\text{DD/DD}}$  rate is independent of potentially varying CSA principal axis values and orientation and constitutes a valuable parameter to investigate anisotropic reorientation of the protein backbone. Nevertheless, due to its small size, the measurement of this rate for small proteins is rather inaccurate in a reasonable measurement time. The analysis of the cross-correlated relaxation data in terms of internal motions consistently deviates from the assumed GAF model. These discrepancies are more evident in  $\beta$ -sheets region and could be explained by CSA changes along the polypeptide chain, which have a large effect on the  $\Gamma_{C', \text{NH}^N}^{\text{CSA/DD}} + \Gamma_{N, C'^\text{H}^N}^{\text{CSA/DD}}$  rate. A

good explanation of the experimental data on the basis of a GAF model could be obtained for turn and coil regions. For  $\alpha$ -helix 23–34, the data could be fitted to the GAF model of motion as well. However, the discrepancies between our results and MD simulation and the regular tendency of all three cross-correlated relaxation rates might indicate either the presence of slow cooperative motion of the helix or considerable deviation of the CSA tensors from their solid-state values. Due to the limited data set available for  $\alpha$ -helices, the question of whether the regularity in the deviation of the rates from their static values in standard geometry can be explained on the basis of large regular changes in physical/structural parameters, by a peculiar type of slow motion of the  $\alpha$ -helix in ubiquitin, or by local fluctuations that are not in accord with the GAF model remains open.

**Acknowledgment.** This work was supported by the Fonds der Chemischen Industrie, the DFG and the MPG. T.C. is supported by the E.U. through a Marie Curie stipend; M.H. acknowledges a Ph.D. fellowship by the Fonds der Chemischen Industrie. The authors thank Dr. B. Geierstanger for helpful discussions and critical reading of the manuscript. All measurements were performed at the large scale facility for Biomolecular NMR as the University of Frankfurt.

**Supporting Information Available:** Trace from the experiment of Figure 3, pictorial representation of Table 4, and a table reproducing the data of Figure 4 (PDF). This material is available free of charge via the Internet at <http://pubs.acs.org>.

JA993845N